In vivo imaging of the human rod photoreceptor mosaic

Nathan Doble,[1,5,*] Stacey S. Choi,[1,5] Johanan L. Codona,[2] Julian Christou,[3] Jay M. Enoch,[4] and David R. Williams[1]

[1]*Center for Visual Science, University of Rochester, Rochester, New York 14627, USA*

[2]*Center for Astronomical Adaptive Optics, Steward Observatory, University of Arizona, 933 North Cherry Avenue, SO N412A, Tucson, Arizona, 85715, USA*

[3]*Gemini Observatory, 670 North A'ohoku Place, Hilo, Hawaii, 96720, USA*

[4]*School of Optometry, University of California, Berkeley, California 94704, USA*

[5]*Currently at the New England College of Optometry, 424 Beacon Street, Boston, Massachusetts 02115, USA*

**Corresponding author: doblen@neco.edu*

Received October 25, 2010; revised November 11, 2010; accepted November 14, 2010; posted November 29, 2010 (Doc. ID 136895); published December 16, 2010

Although single cone receptors have been imaged *in vivo*, to our knowledge there has been no observation of rods in the living normal eye. Using an adaptive optics ophthalmoscope and post processing, evidence of a rod mosaic was observed at 5° and 10° eccentricities in the horizontal temporal retina. For four normal human subjects, small structures were observed between the larger cones and were observed repeatedly at the same locations on different days, and with varying wavelengths. Image analysis gave spacings that agree well with rod measurements from histological data.

OCIS codes: 010.1080, 330.4460, 170.4460.

The earliest efforts to image retinal photoreceptors *in vivo* concentrated on snakes [1] and toads [2], which have good optical quality and large photoreceptors. In the living human eye, the requirement for pupil dilation and the associated aberration increase make visualization of such cells challenging. To fully maximize the resolution and contrast of cellular structures in the human eye, it is necessary to correct all spatial and dynamic aberration variations. Adaptive optics (AO) [3] provide this capability, enabling resolution of single cones [4]. Despite routine cone imaging, to our knowledge there is only one report of imaging of rods *in vivo* in normal human eyes [5], although Carroll *et al.* [6] report imaging of the photoreceptor mosaic in a rod monochromat. Imaging rods will have important applications in the study of retinitis pigmentosa [7] and age-related macular degeneration [8], which often affect these cells first. *In vivo* images of the foveal cones, which are similar in size to rods, have been obtained [9], implying that the rod mosaic should also be observable. Foveal cones have center-to-center (c–c) spacing ranging from 1.9 μm to 3.4 μm, whereas for rods the range is 2.2 μm–3.0 μm [10,11].

Given that the eye has sufficient lateral resolution to image rods, a further challenge is their typical tuning properties (i.e., the Stiles–Crawford effect): the directionality parameter ρ is 0.02 for rods, compared to 0.05 for cones [12], implying that they are less directional. The broader tuning and their much smaller size mean their photon return will be much less than that of surrounding cones.

Four normal subjects (denoted by N1, N2, N3, and N4) between the ages of 19 and 26 years were imaged using the Rochester AO ophthalmoscope [9]. All subjects gave prior written consent in accordance with the Declaration of Helsinki. All had healthy retinas with either mild or no refractive error (3 emmetropes and 1 low myope). Axial lengths (IOL Master—Carl Zeiss Meditec, Dublin, Calif.) and the scaled size of the 1° AO images using Bennett's adjustment [13] are given in Table 1. The subjects' pupils were dilated with one drop of 1% tropicamide followed by one drop of 2.5% phenylephrine prior to AO imaging. To ensure good fixation and to stabilize head movements, a bite bar was used. An image was taken once the AO system reached an rms error value of <0.1 μm over the 6.8 mm exit pupil.

For the retinal location, 5° and 10° in the horizontal, temporal retina (TR) were chosen for several reasons: (i) the image quality degrades with increasing eccentricity owing to increased scatter from the overlying retinal layers; (ii) the cones can be used as physical landmarks, because the cone size and spacing increase with increasing eccentricity, whereas the rod size and spacing stay constant over small excursions (<15°) [10,11]; and (iii) there are fewer overlying nerve fibers.

The contrast of the cone mosaic is wavelength invariant [14], despite the increasing reflectance from the posterior layers at longer wavelengths [15]. This increased reflectance, coupled with a larger permitted input level, requires collection of a smaller number of frames, reducing the effect of camera read noise at the expense of slightly reduced resolution.

The imaging source was a krypton flashlamp with pulse durations of 4 ms delivered through a 1.5 mm entrance pupil. Single pulse energies for the 650 and 750 nm wavelengths were 0.44 and 0.27 μJ, respectively, a factor of 40 below the safety limits [16]. Wavelengths were chosen using interference filters (FWHM of 40 nm) with an estimated coherence length of 8.5–10.5 μm, shorter than the thickness of the retina, reducing the speckle. Prior to imaging, subjects' retinas were bleached using a 10 s exposure of 550 nm light at 37×10^6 Troland seconds, sufficient to bleach 98% of the photopigment [17]. A set of eight images was acquired in the 40 s immediately

Table 1. Axial Lengths and the AO Image Scale

Subject	Axial Length (mm)	1° field in μm [13]
N1	22.98	276.3
N2	23.22	279.5
N3	22.97	276.2
N4	23.24	279.7

afterwards, short enough to ensure that the photopigment had not regenerated [18]. The process was then repeated at the other wavelength. Approximately 50 images were taken at each location for each wavelength, and the best five to seven images were selected for further processing. The imaging camera was mounted on an axial translation stage to correct for the chromatic aberration difference between the AO wavefront sensor (WFS) beacon at 820 nm and the two imaging wavelengths.

For each image frame, the WFS estimate of the 66 Zernike coefficients (ANSI format [19]—10th order) was used to construct the corresponding wavefront aberration profile. Monochromatic light and constant amplitude across the unobstructed 6.8 mm pupil diameter was assumed. By Fourier transforming the retinal image and multiplying by the ideal optical transfer function (OTF) divided by the OTF computed from the residual Zernike coefficients, the residual error and diffraction blur was removed. Where the OTF is much smaller than the ideal value, noise amplification can become an issue. To avoid this, the correction filter was clipped to a maximum complex amplitude while retaining its phase. The resulting filter was applied in the spatial frequency domain and Fourier transformed back to the angular image space.

The resulting images were further enhanced to facilitate analysis. The lower angular-frequency albedo structure was estimated using a Gaussian high-pass filter, adjusted so as to pass the cone and rod spatial frequencies while suppressing the larger variations. Using this filter, the deconvolved image was decomposed into two parts: (i) a low-angular frequency background image and (ii) a high-angular frequency image containing the cones and rods. Examination of the power spectral densities (PSDs) of the averaged images suggested that a power-law enhancement of angular frequency power would bring the rods' visibility in line with that of the cones. The higher spatial frequencies (beyond the rod PSD) had a lower signal-to-noise ratio, and the power-law enhancement would boost this noise source. This was avoided by including a two-dimensional Chebyshev filter adjusted to pass the desired structures, while strongly suppressing the noise-dominated spatial frequencies. Once this was done, and the power normalized to preserve the cones' visibility, the resulting enhanced image was added back to the background, resulting in an enhanced retinal image. All image processing operations are linear in intensity, allowing us to use a correlation registration algorithm [9] that corrected for small shifts between images and removed any torsional eye

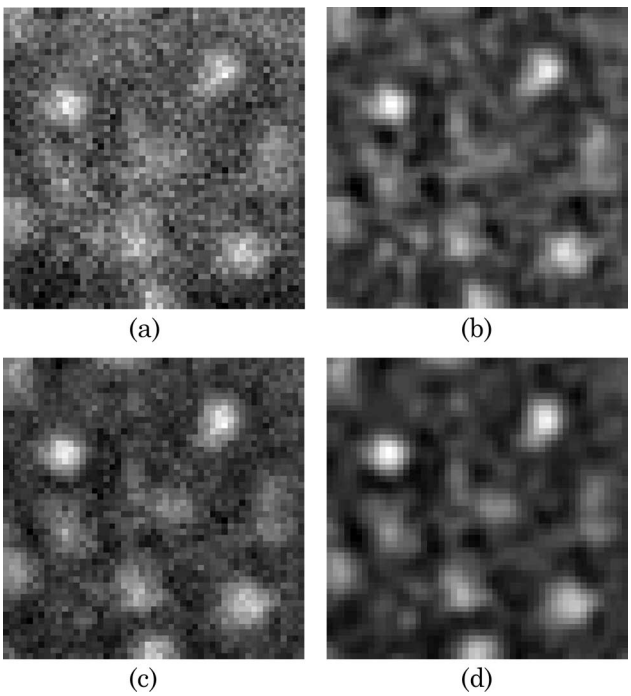

Fig. 1. Retinal images for subject N1, using 650 nm, 10° TR, and field of view (FOV) of 28×28 μm. (a) Dark subtracted, single image frame; (b) deconvolved and filtered image of (a); (c) background subtracted, registered sum of five images; (d) deconvolved image of (c). Rods are observed between the much larger cones, with the same features being observed in the single frame, registered, and enhanced images. The rod c–c spacing of 3.2 ± 0.5 μm agrees well with values from histology. The cone c–c spacing was 9.1 ± 0.9 μm.

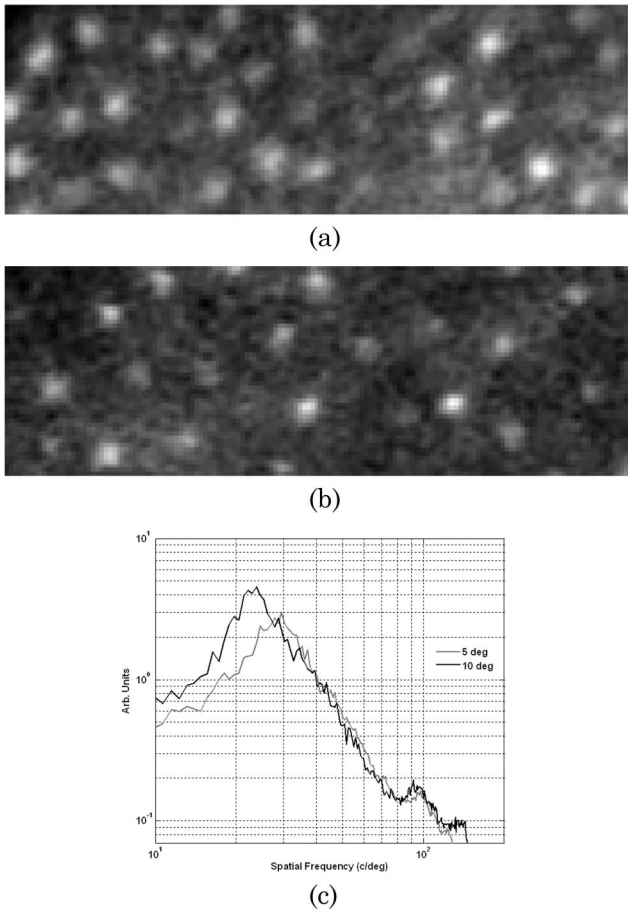

Fig. 2. Enhanced retinal images for subject N2, using 650 nm and FOV of 28×84 μm, registered sum of five images. (a) 5° TR, c–c cone and rod spacings of 9.3 ± 1.7 and 3.1 ± 0.6 μm, respectively; (b) 10° TR, c–c cone and rod spacings of 11.7 ± 1.1 and 3.2 ± 0.3 μm, respectively; (c) PSD from the full 1° image at 5° (gray curve) and 10° (black curve). The cones showed a decrease in spatial frequency with increasing eccentricity giving peak spatial frequencies of 30 and 24 c/deg at 5° and 10°, respectively. The rods showed a similar spatial frequency peak of around 92 c/deg at each retinal location. As expected from histology, the rods' spacing changes only slightly with increasing eccentricity [10,11].

Table 2. Comparison of Measured Photoreceptor c–c Spacing and Histological Data [10,11]

Temporal Eccentricity	Histology		N1		N2		N3		N4	
	4.5°	17°	5°	10°	5°	10°	5°	10°	5°	10°
Cone (c–c) μm	9.4	15.0	7.8	9.1	9.3	11.7	8.9	11.6	7.7	10.3
Rod (c–c) μm	2.2–3.0	2.8	3.2	3.2	3.1	3.2	3.2	2.9	2.3	2.8

motion. Approximately five to seven images were registered and summed.

Figure 1 shows the effect of image processing for subject N1. The same structures can be seen in the single, registered sum, and deconvolved images.

Figure 2 shows enhanced images for subject N2 at 5° and 10° TR at 650 nm. The cones show a decrease in spatial frequency with increasing eccentricity giving peaks at 30 and 24 c/deg at 5° and 10°, respectively. The rods show PSD peak at 92 c/deg for each location.

The mean values (15 rod or cone c–c measurements in each case) for all four subjects at each location are given in Table 2, along with histological comparisons [10,11]. The cone and rod spacings were determined by manual measurement from the 1° AO images. Additionally, PSDs were determined to confirm the cone and rod c–c spacing using the full 1° images.

Speckle [20] is a concern for light sources with high spatial and temporal coherence. The expected speckle size for a 6.8 mm pupil is 1.9 μm at 650 nm, increasing to 2.35 μm at 750 nm. A flashlamp source like the one used here is temporally incoherent, but to ensure that the rod structures were not due to spatial coherence, several parameters were varied. On varying the wavelength, the same structures were observed at the same retinal locations on the same subject; this was also true when the imaging procedure was repeated seven days later. Moreover, the separation of the rods did not change with either wavelength or time. Finally, the diameter of the entrance pupil was varied (1.5–3 mm diameter in 0.5 mm steps); again, the same structures were observed at the same locations with the same separation. As the entrance pupil was increased, a decrease in the cones and rods contrast was observed. This is due to less efficient coupling of the light into the cone receptors and hence increased scatter from the underlying choroidal structures.

Rods were not observed throughout the entire image, however collectively; the results indicate that these are indeed rods. To image them more readily and routinely, further improvements in imaging technology are required, e.g., utilizing pupil plane obscurations centered at the peak of an individual's Stiles–Crawford function to suppress the light from the brighter cones. Utilizing the difference in directional sensitivity between rod and cones and using differential bleaching may also help. Other imaging approaches, such as an adaptive optics confocal laser scanning ophthalmoscope [21], offer improved signal-to-noise and lateral resolution and the potential for averaging many more frames. Because rods are often the first receptors to be damaged in retinal disease, if one can image them as readily as we can image cones, *in vivo* monitoring of rod viability will make an invaluable clinical tool in both diagnosis and therapeutic practice.

The authors thank J. Lin and J. Plandowski for their help. This work has been supported in part by National Eye Institute grants 1RO1EY020901, EY04367, and EY01319 and through the National Science Foundation and Technology—Center for Adaptive Optics, managed by the University of California at Santa Cruz.

References

1. M. F. Land and A. W. Snyder, Vision Res. **25**, 1519 (1985).
2. W. S. Jagger, Vision Res. **25**, 729 (1985).
3. H. W. Babcock, Pub. Astron. Soc. Pacific **65**, 229 (1953).
4. J. Liang, D. R. Williams, and D. T. Miller, J. Opt. Soc. Am. A **14**, 2884 (1997).
5. S. S. Choi, N. Doble, J. Christou, J. Plandowski, J. Enoch, and D. R. Williams, Invest. Ophthalmol. Visual Sci. **45**, 2794 (2004).
6. J. J. Carroll, S. S. Choi, and D. R. Williams, Vision Res. **48**, 2564 (2008).
7. K. R. Alexander and G. A. Fishman, Br. J. Ophthalmol. **68**, 561 (1984).
8. C. A. Curcio, N. E. Medeiros, and C. L. Millican, Invest. Ophthalmol. Visual Sci. **37**, 1236 (1996).
9. N. M. Putnam, H. J. Hofer, N. Doble, L. Chen, J. Carroll, and D. R. Williams, J. Comp. Neurol. **5**, 632 (2005).
10. C. A. Curcio, K. R. Sloan, R. E. Kalina, and A. E. Hendrickson, J. Comp. Neurol. **292**, 497 (1990).
11. J. B. Jonas, U. Schneider, and G. O. H. Naumann, Graefe's Arch. Clin. Exp. Ophthalmol. **230**, 505 (1992).
12. J. M. Enoch and F. L. Tobey, *Vertebrate Photoreceptor Optics*, Springer Series in Optical Sciences (Springer-Verlag, 1981).
13. A. G. Bennett, A. G. Rudnicka, and D. F. Edgar, Graefe's Arch. Clin. Exp. Ophthalmol. **232**, 361 (1994).
14. S. S. Choi, N. Doble, J. Lin, J. Christou, and D. R. Williams, J. Opt. Soc. Am. A **22**, 2598 (2005).
15. F. C. Delori and K. P. Pflibsen, Appl. Opt. **28**, 1061 (1989).
16. International Commission on Non-Ionizing Radiation Protection, Health Phys. **73**, 539 (1997).
17. M. Hollins and M. Alpern, J. Gen. Physiol. **62**, 430 (1973).
18. W. A. H. Rushton and G. H. Henry, Vision Res. **8**, 617 (1968).
19. American National Standard for Ophthalmics, "Methods for Reporting Optical Aberrations of Eyes," ANSI Z80.28-2000 (American National Standards Institute, 2000).
20. J. C. Dainty, *Laser Speckle and Related Phenomena* (Springer-Verlag, 1984), Chap. 7.
21. A. Roorda, F. Romero-Borja, W. J. Donnelly, H. Queener, T. J. Herbert, and M. C. W. Campbell, Opt. Express **10**, 405 (2002).